# Microphase separation-promoted crystallization in all-conjugated poly(3-alkylthiophene) diblock copolymers with high crystallinity and carrier mobility

**6 AUTHORS**, INCLUDING:

Feng Jian Qiu
China University of Geosciences (Beijing)

**135** PUBLICATIONS    **2,307** CITATIONS

**PAPER**

# Microphase separation-promoted crystallization in all-conjugated poly(3-alkylthiophene) diblock copolymers with high crystallinity and carrier mobility†

**Jing Ge,[a] Ming He,[a] Xiubao Yang,[a] Zhi Ye,[a] Xiaofeng Liu[b] and Feng Qiu*[a]**

The crystallinity of all-conjugated diblock copolymer, poly(3-butylthiophene)-*b*-poly(3-dodecylthiophene) (P3BDDT), with varied block ratios was significantly enhanced by a "two-step" thermal annealing treatment. The resulting P3BDDT exhibited an attractively high crystallinity of ~35%, which is a 3-fold enhancement over those of its homopolymer counterparts. The space-charge limited current (SCLC) mobility measurement revealed that the carrier mobility of the highly crystalline P3BDDT film was increased to as high as ~$8.4 \times 10^{-3}$ cm$^2$ V$^{-1}$ s$^{-1}$, exceeding the highest SCLC mobility of poly(3-alkylthiophene) homopolymer films reported in previous work (*i.e.*, ~$1.6 \times 10^{-3}$ cm$^2$ V$^{-1}$ s$^{-1}$). DSC, XRD, AFM and SAXS characterizations demonstrated that the interplay of crystallization and microphase separation during the "two-step" thermal annealing treatment plays a key role in the improvement of P3BDDT crystallinity.

## 1. Introduction

Conjugated polymers have attracted considerable attention due to their promising applications in organic electronic devices, such as organic field-effect transistors (OFETs),[1,2] organic light-emitting diodes (OLEDs)[3,4] and organic photovoltaic cells (OPVs).[5,6] The molecular organization and nanostructure are of importance in optimizing the performance of these semiconducting polymers.[7,8] To precisely control the orientation and nanostructures in conjugated polymer films, one rational way is to design block copolymers composed of dissimilar conjugated blocks, which can self-organize into well-defined microphase-separated domains in the nanoscale dimension,[9,10] driven by immiscibility or a crystallinity difference between the blocks. All-conjugated block copolymers comprised of dissimilar rod-like blocks have become a focus of interest, due to their attractive combination of well-controlled microphase separation, self-assembly and electronic activity of the conjugated blocks.[11] Poly(3-alkylthiophene) (P3AT) and its all-conjugated block copolymers have emerged as very important conjugated polymers in the application of organic devices owing to the excellent solution processability, environmental stability and high carrier mobility.[12–15]

Charge carrier transport is an essential factor in the performance of polymer electronic devices.[1,12–18] The improvement of carrier mobility in P3ATs has been achieved by modifying chemical structures (*i.e.*, the side chain, regioregularity or molecular weight),[1,18,19] by tuning various process parameters (*i.e.*, the solvent boiling point or film deposition method)[13,16,20] and by using various post-treatments (*i.e.*, solvent annealing or thermal annealing).[21] It has been suggested that a highly ordered molecular organization is crucial for enhancing charge carrier transport in polymer devices. Thus, the crystallinity contributes a lot to the enhancement of charge carrier transport in the conjugated polymer films. Further enhancement in crystallinity may lead to a significant improvement of carrier mobility. However, studies on crystallization kinetics revealed that the maximum equilibrium crystallinity of P3AT homopolymers is less than 20% based on the results of differential scanning calorimetry (DSC).[22] The highest space-charge limited current (SCLC) mobility of pristine P3ATs was ~$1.6 \times 10^{-3}$ cm$^2$ V$^{-1}$ s$^{-1}$ as reported in P3BT.[23]

In contrast to simple blending, the chemically bonded blocks in diblock copolymers may be constrained into distinct domains by microphase separation, the domain widths of which are close to the length of the polymer chains. The microphase separation of all-conjugated block copolymers provides the possibility to control the crystallization of one specific block, as the block may be confined within the phase-separated domains or within the previously crystalline stacks of the other block.[11,24] Although a series of all-conjugated P3AT diblock copolymers, including those in our previous work, have been successfully synthesized by the modified Grignard metathesis (GRIM) polymerization,[25–31]

*[a]State Key Laboratory of Molecular Engineering of Polymers, Department of Macromolecular Science, Fudan University, Shanghai 200433, China. E-mail: fengqiu@fudan.edu.cn*

*[b]Department of Chemistry, Fudan University, Shanghai 200433, China*

† Electronic supplementary information (ESI) available: GPC profiles, $^1$H NMR spectra, degrees of crystallization of P3BDDT and SCLC mobility of P3BDDT after the "one-step" thermal treatment. See DOI: 10.1039/c2jm33204c

This journal is © The Royal Society of Chemistry 2012

*J. Mater. Chem.*, 2012, **22**, 19213–19221 | 19213

most of which focused on the crystallization rather than the microphase separation of them,[24] an effective method to tune the relationship between the crystallization and microphase separation of all-conjugated P3AT diblock copolymers is still lacking.

Herein, we report the significantly enhanced crystallinity of all-conjugated poly(3-butylthiophene)-b-poly(3-dodecylthiophene) (P3BDDT) diblock copolymers by a "two-step" thermal annealing treatment. The crystallinity of P3BDDT can be increased to as high as ~35% as compared to that of ~14% in its homopolymer counterparts (i.e., P3BT, P3HT and P3DDT). The SCLC mobility measurement reveals that the carrier mobility of the highly crystalline P3BDDT film can readily reach ~8.4 × $10^{-3}$ cm$^2$ V$^{-1}$ s$^{-1}$, exceeding the highest SCLC mobility of poly(3-alkylthiophene) films reported in previous work (i.e., ~1.6 × $10^{-3}$ cm$^2$ V$^{-1}$ s$^{-1}$). It was demonstrated that the interplay between crystallization and microphase separation during the 'two-step' thermal annealing treatment plays a key role in the improvement of P3BDDT crystallinity, wherein the crystallization of the P3DDT block was largely promoted under the confinement of the previously microphase-separated and crystallized P3BT domains.

## 2. Experimental section

### 2.1 Materials

The monomers, 2-bromo-5-iodo-3-butylthiohpene (M$_1$) and 2-bromo-5-iodo-3-dodecylthiohpene (M$_2$), were synthesized according to the literature.[32] Isopropylmagnesium chloride (2.0 M solution in THF) (i-PrMgCl), [1,3-bis(diphenylphosphino)propane]dichloronickel(II) (Ni(dppp)Cl$_2$) were purchased from Sigma–Aldrich and the other reagents were purchased from Sinopharm Chemical Reagent Co., Ltd. Tetrahydrofuran (THF) was distilled from sodium benzophenone ketyl and all other reagents were used as received. Samples of the P3AT homopolymers (P3BT, P3HT and P3DDT) and three categories of P3BDDT diblock copolymers with varied block ratios were synthesized by a modified GRIM polymerization according to our previous report.[28] All P3BDDT diblock copolymers have comparable number-average molecular weights (M$_n$) in the range of 23 300–27 700, corresponding to about 131–134 thiophene units in the main chains. The homopolymers of P3BT, P3HT and P3DDT as controls have comparable polymerization degrees in the range of 121–159.

### 2.2 Thermal annealing treatments

Thermal annealing treatments were all carried out under argon flux. Films were first melted at 300 °C to eliminate the thermal history. Two different thermal annealing treatments were utilized. One was annealing at 150 °C for 200 min (named the "one-step" thermal annealing), which is commonly used for the thermal annealing of P3ATs.[21,33,34] The other was an initial annealing at 200 °C for 100 min and a subsequent annealing at 110 °C for 100 min (named the "two-step" thermal annealing). For P3BDDTs, a temperature of 200 °C lies in between the melting points (T$_m$) of the P3BT block and P3DDT block, which allows the crystallization of the P3BT block while the P3DDT block remains in the molten state. The P3DDT block crystallizes at a temperature of 110 °C below its T$_m$.

### 2.3 Device fabrication

The space-charge limited current (SCLC) device was fabricated with the architecture of ITO/MoO$_3$/P3BDDT/Ag. The ITO-coated glass substrate was cleaned sequentially by ultra-sonication in acetone, methanol and isopropanol, followed by O$_2$-plasma exposure for 10 min. The MoO$_3$ film (~20 nm) was deposited onto the precleaned ITO substrate by thermal evaporation in a vacuum of 2 × $10^{-6}$ mbar. A 20 mg mL$^{-1}$ P3BDDT chloroform solution was passed through a 0.45 μm filter and then spin-coated on the MoO$_3$ layer at 2000 rpm for 60 s. The "two-step" or "one-step" thermal annealing was performed following the procedure described above. Ag electrodes were deposited by thermal evaporation in a vacuum of 2 × $10^{-6}$ mbar through a shadow mask onto the polymer layer.

### 2.4 Characterization

Gel permeation chromatography (GPC) was operated using an Agilent 1100 system equipped with a UV detector (eluent: THF; calibration: polystyrene standards). $^1$H NMR spectra in CDCl$_3$ were collected on a DMX 500 MHz spectrometer using tetramethylsilane (TMS) as the internal standard. Differential scanning calorimetry (DSC) was performed using TA DSC Q2000 at a heating rate of 10 °C min$^{-1}$ under N$_2$ flow and the transition temperature was derived using TA Universal Analysis Software, which chooses a weighted peak position as the transition temperature. We note that the transition temperature can also be identified by choosing the intersection of the peak at its end with the straight-line heat capacity.[35] X-Ray diffraction (XRD) data were recorded by a PANalytical X'Pert PRO X-ray diffractometer using Cu Kα radiation (λ = 1.541 Å) operating at 40 kV and 40 mA. In situ small angle X-ray scattering (SAXS) experiments were performed at the BL16B1 beam line of Shanghai Synchrotron Radiation Facility (SSRF) in Shanghai, China with a fixed wavelength of 1.24 Å, a sample-to-detector distance of 5 m and an exposure time of 300 s. The 2D scattering patterns were collected on a charge coupled device camera and the curve intensities versus q were obtained by integrating the data from the pattern. Atomic force microscopy (AFM) was performed on a Bruker Multimode AFM Nanoscope IV in tapping mode. The measurements of the SCLC I–V curves were performed using the Keithley 2400 multisource meter. The film thickness was measured by a Bruker Dektak 150 profiler.

## 3. Results and discussion

### 3.1 Synthesis of P3BDDT

Three categories of P3BDDT diblock copolymers with feed molar ratios of 1 : 2, 1 : 1 and 2 : 1, denoted as B34DD66, B49DD51 and B67DD33, were synthesized via quasi-living modified GRIM polymerization. P3AT homopolymers (i.e., P3BT, P3HT and P3DDT) with similar polymerization degrees were also synthesized by the same method (see Experimental section). The synthetic route for P3BDDT is shown in Scheme 1. The P3BT living block was first obtained by the polymerization of GRIM activated M$_1$ with a Ni catalyst and then the GRIM product of M$_2$ was added to obtain the diblock copolymer, P3BDDT. GPC profiles (Fig. S1†) show the increase of the
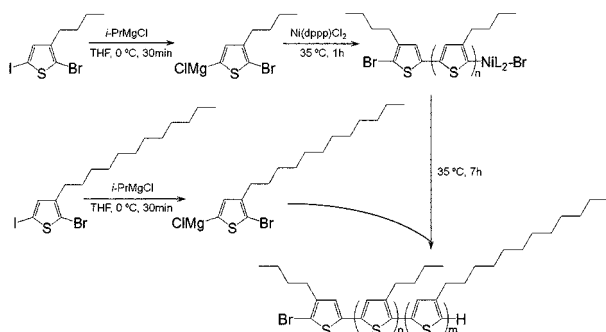
**Scheme 1** Synthesis of poly(3-butylthiophene)-*b*-poly(3-dodecylth-iophene) (P3BDDT).

molecular weight compared to the P3BT block synthesized in the first step, with the maintenance of the single peak, indicating the successful production of P3BDDT with little P3BT contaminant. Three categories of P3BDDT diblock copolymers all show similar $M_n$ values in the range of 23 300–27 700 with narrow polydispersity indices (PDIs) of 1.03–1.11, as shown in Table 1. The molecular weights and PDIs of three P3AT homopolymers are also listed in Table 1. The block compositions of P3BDDT were determined from the $^1$H NMR spectra (Fig. S2†), based on the terminal methyl groups of the butyl and dodecyl side chains, which showed resonances at 0.98 and 0.87 ppm, respectively. The resulting block ratios of P3BDDT are 34 : 66, 49 : 51 and 67 : 33 respectively, which are very close to the feed molar ratios of 1 : 2, 1 : 1 and 2 : 1 (Table 1). Based on the results of the molecular weights and compositions, the degree of polymerization of the P3BDDT diblock copolymers was evaluated to be about 131–134 thiophene units in the main chains. The homopolymers of P3BT, P3HT and P3DDT as controls have comparable polymerization degrees in the range of 121–159. These GPC and $^1$H NMR results demonstrate the successful synthesis of P3BDDT with relatively high molecular weights, narrow PDIs and controllable compositions by quasi-living modified GRIM polymerization. We note that few tri-block copolymers may also be obtained due to the possible random walk of the catalyst based on the latest investigations.[36]

## 3.2 Thermal analysis

The thermal analysis of as-synthesized P3BDDT diblock copolymers was performed by DSC measurements. All samples

were heated at 300 °C for 10 min to eliminate the thermal history, followed by cooling and heating scans at the rate of 10 °C min$^{-1}$. The cooling and heating traces of P3BDDT diblock copolymers with varied block ratios are shown in Fig. 1. Two distinct crystallization and melting peaks emerge during the cooling/heating process, which correspond well to those of P3BT and P3DDT blocks (Fig. 1a and b), suggesting the occurrence of microphase separation induced by the independent crystallization of each block.[28] Fig. 2 shows the crystallization temperature ($T_c$) and melting point ($T_m$) of the P3BT block and P3DDT block as a function of the block ratio. For the P3BT block (Fig. 2a), both $T_c$ and $T_m$ decrease with an increase of the P3DDT block ratio. This phenomenon can be ascribed to two reasons: (1) $T_c$ and $T_m$ values can be affected by molecular weight below a critical value.[38] (2) Due to their similar chemical structures, P3BT and P3DDT blocks are expected to be miscible in the molten state. Therefore, the P3DDT block with longer alkyl side chains can act as a diluent, depressing the $T_c$ and $T_m$ of the P3BT block, which also has been reported in the crystallization of block copolymers from a disordered melt.[39–41] Hence, both the diluent effect and molecular weight account for the depression of the crystallization and melting temperatures of the P3BT block within P3BDDT diblock copolymers. For the P3DDT block, its $T_c$ values remain in the range very close to that of the P3DDT homopolymer and the $T_m$ values lie in the range slightly higher than that of the P3DDT homopolymer (Fig. 2b), indicating that the preferentially crystallized P3BT block may probably promote, rather than restrict, the subsequent crystallization of the P3DDT block.[38] We note that the broaden $T_c$ peak and inflection in the DSC heating scan of B34DD66 may be induced by the
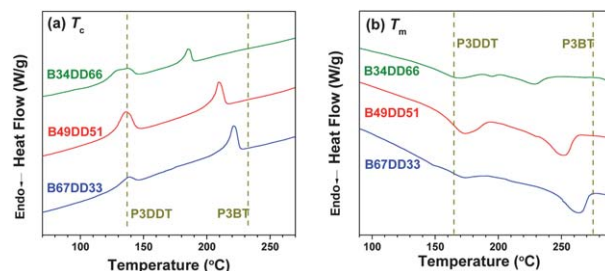


**Fig. 1** DSC (a) cooling scans and (b) heating scans of B34DD66, B49DD51 and B67DD33. The vertical dashed lines indicate the corresponding temperature of P3DDT and P3BT homopolymers, respectively.

**Table 1** Summary of the molecular weights and compositions of poly(3-butylthiophene) (P3BT), poly(3-hexylthiophene) (P3HT), poly(3-dodecylth-iophene) (P3DDT) and poly(3-butylthiophene)-*b*-poly(3-dodecylthiophene) (P3BDDT) with three varied block ratios

| Polymers | Feed molar ratio[a] | $M_n$ (g mol$^{-1}$) | PDIs | $n/m$[b] (%) | $f_{P3DDT}$[c] | Denotation[d] |
|---|---|---|---|---|---|---|
| P3BT | 1 : 0 | 22 000 | 1.12 | 100 : 0 | — | — |
| P3HT | 1 : 0 | 20 200 | 1.20 | 100 : 0 | — | — |
| P3DDT | 1 : 0 | 35 400 | 1.09 | 100 : 0 | — | — |
| P3BDDT | 1 : 2 | 27 700 | 1.11 | 34 : 66 | 0.78 | B34DD66 |
|  | 1 : 1 | 26 100 | 1.11 | 49 : 51 | 0.65 | B49DD51 |
|  | 2 : 1 | 23 300 | 1.03 | 67 : 33 | 0.47 | B67DD33 |

[a] Refers to the feed molar ratio of the monomers of the first block and the second block. [b] Determined by $^1$H NMR. *n*, *m*: the molar amount of the first and the second block in the synthesized poly(3-alkylthiophene) diblock copolymers, respectively. [c] Calculated according to the molecular weights, compositions, crystallinity and amorphous densities of each diblock copolymer.[37] [d] Denoted according to the molar ratio of the blocks.
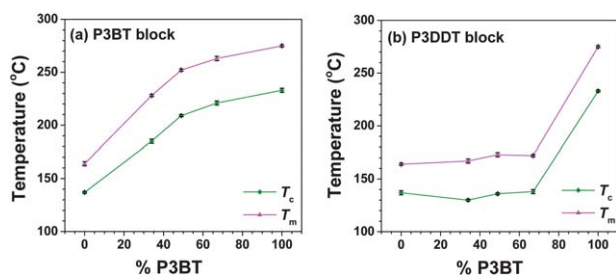
**Fig. 2** Crystallization and melting temperatures of (a) the P3BT block and (b) the P3DDT block within all P3BDDT diblock copolymers as a function of the P3BT block ratio.

fractionated crystallization of the P3DDT block due to its confined crystallization within the micro-domain structures, leading to the crystallization of P3DDT at different supercoolings.[38]

### 3.3 Thermal annealing treatments

Thermal annealing is a useful method to manipulate the molecular organization and nanoscale structure of semiconducting polymers.[34,42] The conventional thermal annealing for P3AT is carried out at 150 °C,[34] named the "one-step" thermal annealing. Based on the independent crystallization characteristic of the two blocks in P3BDDT, a "two-step" thermal annealing procedure tailored to these crystalline–crystalline all-conjugated poly(3-alkylthiophene) block copolymers was utilized. The two steps include the isothermal crystallization of the P3BT block at a high temperature, which allows the maximum crystallization of the P3BT block while the P3DDT block remains in the molten state, and a subsequent isothermal crystallization of the P3DDT block at a relatively low temperature for the maximum crystallization of the P3DDT block. In this work, the first step was performed at 200 °C, which is lower than the melting point of the P3BT block but higher than that of the P3DDT block. The second step was conducted at 110 °C, which is below the melting point of the P3DDT block. As controls, the "two-step" thermal annealing treatments for P3AT homopolymers were carried out in the same way. The crystallinity, $X$, of P3AT is calculated from $X = \Delta H_m / \Delta H_m^0$,[43] where $\Delta H_m$ is the specific enthalpy of melting of the samples obtained from the heating scan of the DSC measurement and $\Delta H_m^0$ is the specific enthalpy of melting of ideal crystals of P3AT. The values of $\Delta H_m^0$ are 99 and 52 J g$^{-1}$ for P3HT and P3DDT, respectively.[22] The $\Delta H_m^0$ value of P3BT is estimated to be 107.8 J g$^{-1}$ based on the rule of the linear change of $\Delta H_m^0$ values with respect to the number of carbon atoms in the side chain.[22] Then, the crystallinity of P3BDDT is the summation of the crystallinity of the P3BT block ($X_B$) and the PDDT block ($X_{DD}$), which are calculated from $X_B = \Delta H_{m(B)} / (\Delta H_m^0 \cdot w_B)$ and $X_{DD} = \Delta H_{m(DD)} / (\Delta H_m^0 \cdot w_{DD})$, respectively, where $\Delta H_{m(B)}$ and $\Delta H_{m(DD)}$ are obtained from the melting peaks in the DSC scan assigned to the P3BT block and P3DDT block, respectively. Here, $w$ is the weight percent of the block in P3BDDT. It is worth noting that the crystallinity of P3AT also depends on the polydispersity and molecular weight.[44] Therefore, the polydispersity and molecular weight of the P3BDDT block copolymers used in this work are nearly the same in each group (see Experimental

section), in order to reconcile the contribution from the molecular weight and polydispersity.

Fig. 3 shows the crystallinity of the B49DD51 diblock copolymer and P3AT homopolymers after the "one-step" and "two-step" thermal annealing. After the "one-step" thermal annealing, the crystallinity of the P3ATs is larger in the P3AT homopolymer with a shorter alkyl side chain, since the longer side chain may depress the close stacking of the main chain. Quite interesting, the P3BDDT diblock copolymer shows a slightly higher crystallinity (∼20%) over that of the P3ATs (∼17%), indicating that the crystalline behavior depends not only on the length of the side chains but also on the neighboring blocks in all-conjugated P3AT diblock copolymers.[24,38] The "two-step" method can take full advantage of the neighboring block effect,[24] since it enables the previous crystallization of the P3BT block with the P3DDT block in the flexible molten state and the subsequent crystallization of P3DDT. After the "two-step" thermal annealing, all the three categories of P3BDDT show obviously higher crystallinity than the polymer treated by the "one-step" thermal annealing (Fig. S3†). In particular, the highest crystallinity of ∼35% is achieved in B34DD66, which is 3-fold enhancement over that of the P3ATs (∼14%), after the "two-step" thermal annealing. In addition, it has been reported that the crystallinity values determined by other methods (such as extraction from NMR and WAXS data) are significantly larger than that derived from DSC data.[45] We also measured the $T_c$ and $T_m$ values of B34DD66 at varying DSC scan rates (i.e., 20 °C min$^{-1}$, 10 °C min$^{-1}$, 5 °C min$^{-1}$ and 2 °C min$^{-1}$), which revealed that the transition temperature values measured at a scan rate of 10 °C min$^{-1}$ do not represent the equilibrium values (Fig. S4 in the ESI†).[22] The $T_c$ of B34DD66 approaches ∼200 °C when the DSC scan rate is decreased. The equilibrium $T_c$ of ∼201 °C can be derived by extrapolation.

### 3.4 XRD studies

The crystalline structures of the P3BDDT films as well as the P3AT homopolymer films after the "one-step" or "two-step" thermal annealing were characterized by XRD measurements. In order to eliminate the influence of the film thickness, the obtained XRD spectra (shown in Fig. 4) were normalized by the thickness of the films. In the case of the "two-step" treatment, the XRD patterns of the P3BT block and the P3DDT block in P3BDDT both show recognizable first-, second- and third-order reflections from crystallographic (100), (200) and (300) planes, respectively.
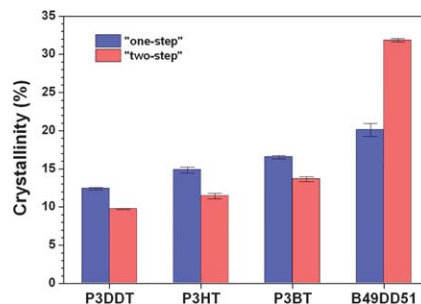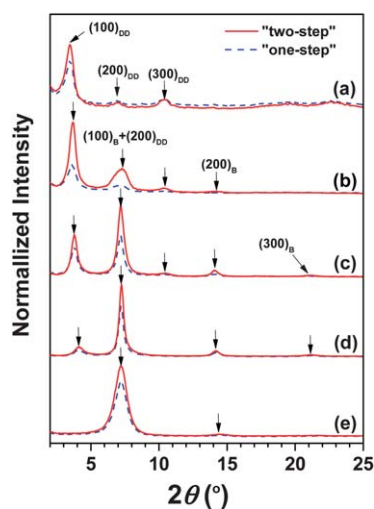


**Fig. 3** Crystallinity in three homopolymers and the B49DD51 block copolymer after the "one-step" or "two-step" thermal annealing.

**Fig. 4** XRD spectra of (a) P3DDT, (b) B34DD66, (c) B49DD51, (d) B67DD33 and (e) P3BT after the "two-step" or "one-step" thermal annealing treatment.

For B34DD66, the diffraction peaks located at $2\theta$ angles of 3.74°, 7.54° and 10.46° correspond to the (100), (200) and (300) reflections of the P3DDT block, respectively (denoted as $(100)_{DD}$, $(200)_{DD}$ and $(300)_{DD}$ in Fig. 4) and the diffraction peaks located at $2\theta$ angles of 7.54° and 14.21° correspond to the (100) and (200) reflections of the P3BT block, respectively (denoted as $(100)_B$ and $(200)_B$ in Fig. 4). This phenomenon demonstrates that the P3BT block and P3DDT block in B34DD66 independently crystallize into two microphase-separated domains with high degrees of microcrystalline order and well-organized lamellar structures, which is similar to what has been reported for B54DD46 by us previously.[28] We note that the $(200)_{DD}$ peak overlaps the peak of $(100)_B$, resulting in a rather broad peak and the (300) reflections of the P3BT block (denoted as $(300)_B$) is not observed due to the minority content of the P3BT block in B34DD66. Based on the $(100)_{DD}$ and $(100)_B$ peaks, the interlayer spacing of the P3DDT block ($d_{100(DD)}$) and P3BT block ($d_{100(B)}$) are 23.7 Å and 11.7 Å, respectively. The $d_{100(B)}$ value (11.7 Å) of the P3BT block is close to that (12.3 Å) of the P3BT homopolymer,[28] implying that the presence of P3DDT block does not impede the crystallization of the P3BT block. The $d_{100(DD)}$ value (23.7 Å) of P3DDT block is a little bit smaller than that (25.8 Å) of the P3DDT homopolymer,[28] indicating the close lamellar packing of the P3DDT block driven by the previously crystallization of the P3BT block and the probable occurrence of tilting of the dodecyl side chains.[46] These results further demonstrate that the previous crystallization of the P3BT block is not impeded by the flexible P3DDT block and, in turn, promotes the subsequent crystallization of the P3DDT block. For B49DD51 and B67DD33, the situations are similar to B34DD66. The $d_{100(DD)}$ and $d_{100(B)}$ values in B49DD51 are 23.5 and 12.3 Å according to the $(100)_{DD}$ and $(100)_B$ diffraction peaks at $2\theta$ angles of 3.77° and 7.21°, respectively. The $(100)_{DD}$ and $(100)_B$ diffraction peaks of B67DD33 lie at $2\theta$ angles of 4.08° and 7.26°, corresponding to the $d_{100(DD)}$ and $d_{100(B)}$ values of 21.6 and 12.2 Å, respectively. As for the "one-step" treatment, the peak positions in the XRD spectra of P3BDDT are similar to the

"two-step" method; however, the peak intensities are different (Fig. 4). Given that the XRD spectra were normalized by the film thickness, the diffraction peak intensity is proportional to the crystallinity. The decrease of the peak intensity in P3BDDT after the "one-step" treatment indicates a decrease in crystallinity compared to after the "two-step" treatment, which coincides with the result shown in Fig. S3.† Therefore, all these results further indicate that P3BDDT can self-organize into a well-organized lamellar crystalline structure with significantly high crystallinity by "two-step" thermal annealing.

### 3.5 AFM images

To investigate the nanoscale morphology of P3BDDT, thin films of B34DD66, B49DD51 and B67DD33 were prepared by spin-coating from toluene solutions and then measured by AFM after the "two-step" thermal annealing. The height images of all samples showed a blurred pattern (Fig. 5a, c and e). On the contrary, their phase images all showed clear microphase-separated nanopatterns after the "two-step" thermal annealing: B34DD66 shows a locally oriented lamellar-like structure with a lamellar width of $15 \pm 5$ nm (Fig. 5b); B49DD51 shows a less ordered lamellar-like structure with a lamellar width of $17 \pm 5$ nm (Fig. 5d); B67DD33 exhibits disordered short-lamellar aggregates with a lamellar width of $14 \pm 2$ nm (Fig. 5f).

The phase behavior of all-conjugated P3BDDT diblock copolymers may be similar to those of rod–coil block copolymers when thermal annealed at 200 °C, as P3BT blocks are in the crystalline state while the P3DDT blocks are in the coil molten state at this temperature. The phase behavior of rod–coil block copolymers is mainly determined by the microphase separation between the crystalline blocks and the coil blocks, as well as the interplay between the crystalline blocks. Olsen and co-workers universalized the phase diagram for the general class of rod–coil
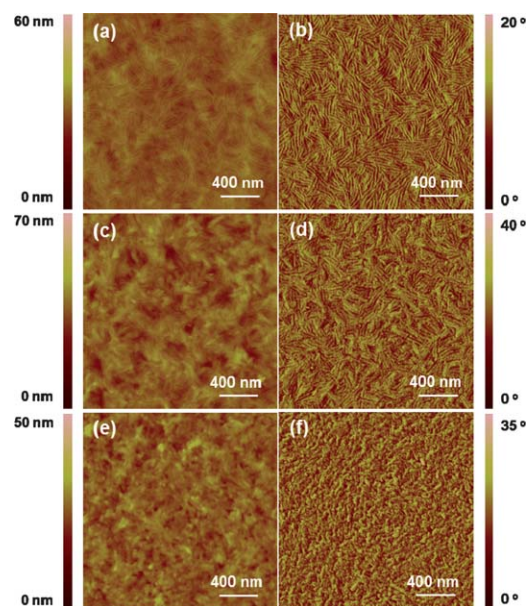


**Fig. 5** AFM (a, c and e) height and (b, d and f) phase images of (a and b) B34DD66, (c and d) B49DD51 and (e and f) B67DD33 after the "two-step" thermal annealing.

block copolymers,[47] from which it can be deduced that our P3BDDT, with the coil fraction in the range of 47% to 78%, would form the lamellar phase at 200 °C. Furthermore, Matsen and Barrett carefully charted the morphology of rod–coil block copolymers in the lamellar phase.[48] According to the phase diagram reported by them, we can expect that our P3BDDT, with the coil fraction in the range of 47% to 78%, would span the smectic A-to-smectic C transition. For decisively characterizing the bulk microphase-separated structure of rod–coil block copolymers, TEM is one of the most widely used methods to directly reveal the phase morphology of the specific sample prepared by ultramicrocut methods. Owing to the low contrast between the P3BT and P3DDT domains, it is still a challenge for us to get high-quality images to illustrate the bulk phase structures of P3BDDT.

### 3.6 SCLC carrier mobility

To investigate the effect of the crystallinity on the charge carrier transport properties, hole-only SCLC devices were fabricated to measure the carrier mobility of the P3BDDT films with varied block ratios after the "two-step" or "one-step" thermal annealing. The hole mobility values were calculated from the current density–voltage (J–V) curves (Fig. 6) that were fitted by applying the modified Mott–Gurney equation:[49]

$$J = \frac{9}{8}\varepsilon\varepsilon_0\mu\frac{V^2}{L^3}\exp\left(\frac{0.89\beta}{\sqrt{L}}\sqrt{V}\right),$$

where $J$ is the current density, $V$ is the applied voltage, $L$ is the thickness of active layer, $\mu$ is the mobility, $\varepsilon$ is the dielectric constant, $\varepsilon_0$ is the permittivity of free space ($8.85 \times 10^{-12}$ F m$^{-1}$) and $\beta$ is the field-activation factor.[49] The dielectric constant, $\varepsilon$, is supposed to be 3 in the calculation.[50]

The mobility, $\mu$, of the P3BDDT and P3AT films after the "two-step" thermal annealing treatment are listed in Table 2. The $\beta$ values of both P3BDDT and the P3ATs are negative, indicating the negative electric field dependence of their hole mobility, which has already been observed in P3HT[51,52] and other P3AT-based blends.[39,43] The carrier mobility of P3BDDT is calculated to be in the range of $3.6 \times 10^{-3}$ to $8.4 \times 10^{-3}$ cm$^2$



**Fig. 6** J–V curves of the space-charge limited current (SCLC) devices for the carrier mobility measurement in P3BDDT with varied block ratios (B34DD66, B49DD51 and B67DD33) and three P3AT homopolymers (i.e., P3BT, P3HT and P3DDT) after the "two-step" thermal annealing. The inset shows the SCLC device architecture.

**Table 2** Summary of the parameters extracted from the J–V curves shown in Fig. 6 according to the Mott–Gurney equation and their crystallinity after the "two-step" thermal annealing process

| Polymer | Mobility $\mu$ (cm$^2$ V$^{-1}$ s$^{-1}$) | Crystallinity (%) |
|---|---|---|
| B67DD33 | $8.4 \pm 0.2 \times 10^{-3}$ | $29.1 \pm 0.2$ |
| B49DD51 | $3.6 \pm 0.1 \times 10^{-3}$ | $31.8 \pm 0.2$ |
| B34DD66 | $5.2 \pm 0.2 \times 10^{-3}$ | $34.8 \pm 0.2$ |
| P3BT | $1.5 \pm 0.2 \times 10^{-3}$ | $13.6 \pm 0.3$ |
| P3HT | $7.6 \pm 0.1 \times 10^{-4}$ | $11.4 \pm 0.3$ |
| P3DDT | $5.8 \pm 0.1 \times 10^{-4}$ | $9.7 \pm 0.1$ |

V$^{-1}$ s$^{-1}$ and, for the P3ATs, it is in the range of $5.8 \times 10^{-4}$ to $1.5 \times 10^{-3}$ cm$^2$ V$^{-1}$ s$^{-1}$ (Table 2). Among the P3AT homopolymers, P3BT shows the highest hole mobility (Table 2), which coincides with the tendency towards crystallinity. The mobility value of the P3BT film ($\sim 1.5 \times 10^{-3}$ cm$^2$ V$^{-1}$ s$^{-1}$) is in good agreement with the reported one for P3BT ($\sim 1.6 \times 10^{-3}$ cm$^2$ V$^{-1}$ s$^{-1}$).[23] The mobility of all P3BDDT diblock copolymers with varied block ratios is higher than that of the P3AT homopolymers. The highest mobility value of B67DD33 ($\sim 8.4 \times 10^{-3}$ cm$^2$ V$^{-1}$ s$^{-1}$) is at least 5-fold higher than that of P3BT ($\sim 1.6 \times 10^{-3}$ cm$^2$ V$^{-1}$ s$^{-1}$). It can be concluded that the enhanced crystallinity of P3BDDT results in the significant improvement of its carrier mobility. The mobility of P3BDDT after the "one-step" thermal annealing is calculated to be in the range of $1.8 \times 10^{-3}$ to $2.9 \times 10^{-3}$ cm$^2$ V$^{-1}$ s$^{-1}$ (shown in Table S1†). The P3BDDT thin films after the "two-step" thermal annealing showed higher mobility than those after the "one-step" thermal annealing, which is in accordance with the tendency towards crystallinity. This result further confirms the impact of crystallinity on the charge carrier transport in poly(3-alkylthiophene) diblock copolymer systems.

### 3.7 Mechanism of crystallinity enhancement

It is crucial to elucidate the mechanism for the generation of significantly high crystallinity via the "two-step" thermal annealing. SAXS measurements were performed on B34DD66 in situ, wherein the SAXS profiles were collected at 300 °C after an isotherm for 10 min, 200 °C after an isotherm for 100 min and 110 °C after an isotherm for 100 min. The SAXS results are shown in Fig. 7. After the elimination of the thermal history (at 300 °C for 10 min), no scattering peak was observed, indicating the uniform miscible disordered melt phase of B34DD66, which is also evidenced by the melting point depression of the P3BT block in P3BDDT. After the first-step thermal annealing (the crystallization of the P3BT block at 200 °C for 100 min), an obvious reflection peak appears at a scattering vector of 0.24 nm$^{-1}$, suggesting the occurrence of microphase separation with a domain spacing of $\sim$26.1 nm. After the second-step of the thermal annealing (the subsequent crystallization of the P3DDT block at 110 °C for 100 min), the position of the reflection peak remains at 0.24 nm$^{-1}$, while the peak intensity decreases compared to that in the previous step. The preservation of the peak position implies that the microphase-separated domain spacing is not disturbed by the subsequent crystallization of the P3DDT block (i.e., the P3DDT block crystallizes within its microphase-separated domain). Since the scattering intensity is
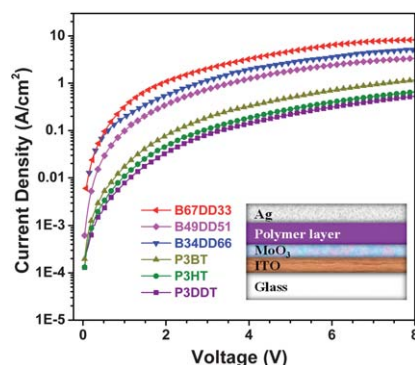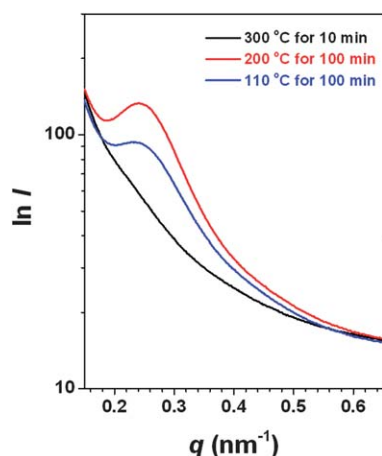
**Fig. 7** SAXS profiles of B34DD66 collected at 300 °C after an isotherm for 10 min, 200 °C after an isotherm for 100 min and 110 °C after an isotherm for 100 min.

proportional to the electron density difference between the two microphase-separated domains,[53] the crystallization of the P3DDT block should cause a decrease in the electron density contrast between the two crystallized domains, as compared to that between the crystallized and the melting domains in the previous step. Therefore, the scattering intensity in the second-step is weaker than in the first-step. It is noteworthy that the single primary peak observed in the P3BDDT SAXS profile is in agreement with the results for the P3BOT block copolymers reported by Wu and co-workers.[27] Our SAXS result is also consistent with the Fourier transform result of the lamellar-like AFM images (e.g., Fig. 5b and Fig. S5 in the ESI†), suggesting that the study of the film in this work may be representative of the bulk properties. The possible reason for the lack of a higher order refection in the SAXS result is still not very clear. One possible explanation is that there are less ordered structures in the large scales due to the weakly segregated P3BT and P3DDT blocks.

Based on the results of DSC, XRD, AFM and SAXS, a possible mechanism for the generation of significantly high crystallinity in P3BDDT via the "two-step" thermal annealing was qualitatively elucidated and is schematically shown in Scheme 2. In the molten state (T = 300 °C), P3BT and P3DDT
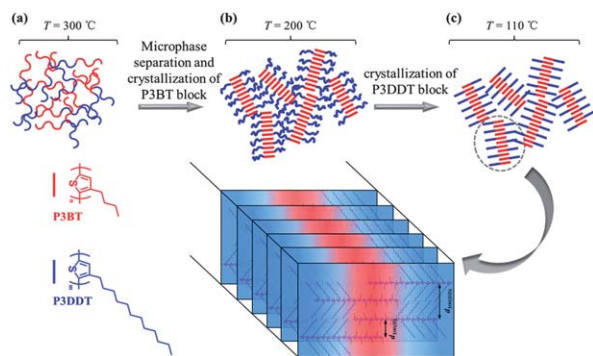


**Scheme 2** Sketch of the possible mechanism for P3BDDT to achieve high crystallinity via the "two-step" thermal annealing.

blocks in P3BDDT are in the miscible coil state (Scheme 2a) due to the chemical similarity of the two blocks, evidenced by the melting point depression of the P3BT block in P3BDDT and the SAXS profile without a diffraction peak at 300 °C. During the first-step thermal annealing at 200 °C, the P3BT block crystallizes, while the P3DDT block remains in a coiled conformation due to its low melting point. The P3BT block tends to form a well-organized lamellar crystalline structure at this stage. As a result, P3BDDT is composed of crystallized domains of the P3BT block and collective domains of the molten P3DDT block after the first-step thermal annealing (Scheme 2b). In the second-step thermal annealing process at 110 °C, the crystallization of the P3DDT blocks occurs within its microphase-separated domain confined by the previously completely crystallized P3BT blocks. As the P3DDT blocks were collected in a confined domain and enabled order to some extent, their crystallization is promoted to produce relatively high crystallinity and a more closely crystalline structure as compared to their P3DDT homopolymer. Therefore, P3BDDT self-organizes into two microphase-separated domains composed of the well-organized lamellar crystalline structure of the two blocks (Scheme 2c) to give a significantly enhanced crystallinity. It is worth noting that the crystallinity of the P3AT homopolymers increased inversely with the side chain lengths (Fig. 3), because a shorter side chain may facilitate the ordered packing of the P3AT chains. Quite interesting, the crystallinity of the diblock copolymer decreases with an increasing content of short P3BT blocks (Fig. S3†). As shown in Fig. S6,† the crystallinities of the P3BT blocks in each P3BDDT block copolymer (i.e., B34DD66, B49DD51 and B67DD33) are comparable, while the crystallinities of the P3DDT blocks in P3BDDT increase with an increasing content of P3DDT blocks, which is ascribed to the confined crystallization within the microphase-separated domains induced by the previous crystallization of the P3BT blocks in the first-annealing step.

We further calculated the crystalline size of the P3BT blocks according to the basic theory developed by J. D. Hoffman and J. I. Lauritzen:[54]

$$\frac{T_m}{T_m^0} = \left(1 - \frac{2\Delta\gamma}{l\Delta H_c}\right),$$

where $T_m$ is the melting temperature, $T_m^0$ is the equilibrium melting temperature, $\Delta\gamma$ is the fold surface free energy per unit area, $l$ is the crystalline lamellae thickness and $\Delta H_c$ is the enthalpy of fusion of the crystals per unit volume. The crystalline lamellae thickness of the crystallized P3BT blocks is calculated to be ~13.4 nm (Table S2 in ESI†). Compared to the B34DD66 domain spacing of ~26.1 nm measured by SAXS at 200 °C, the crystallized P3BT domains occupy nearly 51% of the microphase separated period, which is larger than the volume fraction of the P3BT block (i.e., $f_{P3BT}$ of ~0.22) in the B34DD66 diblock copolymer, suggesting that the crystalline lamellae would first set the size of the P3BT microdomain, which in turn sets the repeat spacing for the microphase separated structure. We note that the folding of the P3AT chains can be inferred from the evolution of the lamellar period with increasing molecular weight, as well as the degree of polymerization.[55] Fig. S7† shows the plot of the melting temperature of each block in the P3BDDT block copolymers versus the degree of polymerization, suggesting the

possible fully extended P3BT chains and the folding of the P3DDT chains in their respectively crystalline domains.[55] The detailed folding of the chains in the P3BDDT block copolymers still needs further exploring, which will be the subject of our future work.

## 4. Conclusions

A significant enhancement of crystallinity and carrier mobility was achieved in a crystalline–crystalline all-conjugated poly(3-alkyllthiophene) diblock copolymer, P3BDDT, by a "two-step" thermal annealing treatment. The crystallinity of P3BDDT was significantly enhanced to ∼35%, as compared to that of ∼14% in its homopolymer counterparts. The SCLC mobility of P3BDDT was dramatically enhanced to ∼8.4 × 10$^{-3}$ cm$^2$ V$^{-1}$ s$^{-1}$, compared to the highest reported value of ∼1.6 × 10$^{-3}$ cm$^2$ V$^{-1}$ s$^{-1}$ in P3AT homopolymers. It was demonstrated that the interplay of crystallization and microphase separation during the 'two-step' thermal annealing treatment plays a key role in the improvement of P3BDDT crystallinity, that is: (1) the molten P3DDT block and the crystallized P3BT block form in the microphase separation during the preferential crystallization of the P3BT block at 200 °C and (2) the crystallization of P3DDT block at 110 °C is largely promoted by the confinement of P3BT-crystalline phases. This strategy of tuning the behaviour of crystallization and microphase separation for high crystallinity or fantastic properties may be extended to other all-conjugated diblock copolymers. Further investigation of the effect of such extraordinary high crystallinity on the performance of other polymer electronic devices is underway.

## Acknowledgements

## Notes and references

1 H. Sirringhaus, P. J. Brown, R. H. Friend, M. M. Nielsen, K. Bechgaard, B. M. W. Langeveld-Voss, A. J. H. Spiering, R. A. J. Janssen, E. W. Meijer, P. Herwig and D. M. de Leeuw, *Nature*, 1999, **401**, 685.
2 B. S. Ong, Y. L. Wu, P. Liu and S. Gardner, *J. Am. Chem. Soc.*, 2004, **126**, 3378.
3 A. C. Grimsdale, K. L. Chan, R. E. Martin, P. G. Jokisz and A. B. Holmes, *Chem. Rev.*, 2009, **109**, 897.
4 M. Gross, D. C. Muller, H. G. Nothofer, U. Scherf, D. Neher, C. Brauchle and K. Meerholz, *Nature*, 2000, **405**, 661.
5 S. Gunes, H. Neugebauer and N. S. Sariciftci, *Chem. Rev.*, 2007, **107**, 1324.
6 K. M. Coakley and M. D. McGehee, *Chem. Mater.*, 2004, **16**, 4533.
7 J. F. Chang, B. Q. Sun, D. W. Breiby, M. M. Nielsen, T. I. Solling, M. Giles, I. McCulloch and H. Sirringhaus, *Chem. Mater.*, 2004, **16**, 4772.
8 H. C. Yang, T. J. Shin, Z. N. Bao and C. Y. Ryu, *J. Polym. Sci., Part B: Polym. Phys.*, 2007, **45**, 1303.
9 M. Lee, B. K. Cho and W. C. Zin, *Chem. Rev.*, 2001, **101**, 3869.
10 I. W. Hamley, *Nanotechnology*, 2003, **14**, R39.
11 M. He, F. Qiu and Z. Q. Lin, *J. Mater. Chem.*, 2011, **21**, 17039.
12 H. Sirringhaus, N. Tessler and R. H. Friend, *Science*, 1998, **280**, 1741.
13 H. C. Yang, T. J. Shin, L. Yang, K. Cho, C. Y. Ryu and Z. N. Bao, *Adv. Funct. Mater.*, 2005, **15**, 671.
14 G. Q. Ren, P. T. Wu and S. A. Jenekhe, *Chem. Mater.*, 2010, **22**, 2020.
15 J. Y. Liu, D. Haynes, C. Balliet, R. Zhang, T. Kowalewski and R. D. McCollough, *Adv. Funct. Mater.*, 2012, **22**, 1024.
16 Z. Bao, A. Dodabalapur and A. J. Lovinger, *Appl. Phys. Lett.*, 1996, **69**, 4108.
17 Z. N. Bao, Y. Feng, A. Dodabalapur, V. R. Raju and A. J. Lovinger, *Chem. Mater.*, 1997, **9**, 1299.
18 Y. D. Park, D. H. Kim, Y. Jang, J. H. Cho, M. Hwang, H. S. Lee, J. A. Lim and K. Cho, *Org. Electron.*, 2006, **7**, 514.
19 R. J. Kline, M. D. McGehee, E. N. Kadnikova, J. S. Liu and J. M. J. Frechet, *Adv. Mater.*, 2003, **15**, 1519.
20 H. H. Yang, S. W. LeFevre, C. Y. Ryu and Z. N. Bao, *Appl. Phys. Lett.*, 2007, **90**, 172116.
21 A. Zen, J. Pflaum, S. Hirschmann, W. Zhuang, F. Jaiser, U. Asawapirom, J. P. Rabe, U. Scherf and D. Neher, *Adv. Funct. Mater.*, 2004, **14**, 757.
22 S. Malik and A. K. Nandi, *J. Polym. Sci., Part B: Polym. Phys.*, 2002, **40**, 2073.
23 G. H. Lu, H. W. Tang, Y. A. Huan, S. J. Li, L. G. Li, Y. Z. Wang and X. N. Yang, *Adv. Funct. Mater.*, 2010, **20**, 1714.
24 X. H. Yu, H. Yang, S. P. Wu, Y. H. Geng and Y. C. Han, *Macromolecules*, 2012, **45**, 266.
25 K. Ohshimizu and M. Ueda, *Macromolecules*, 2008, **41**, 5289.
26 Y. Zhang, K. Tajima, K. Hirota and K. Hashimoto, *J. Am. Chem. Soc.*, 2008, **130**, 7812.
27 P. T. Wu, G. Q. Ren, C. X. Li, R. Mezzenga and S. A. Jenekhe, *Macromolecules*, 2009, **42**, 2317.
28 J. Ge, M. He, F. Qiu and Y. L. Yang, *Macromolecules*, 2010, **43**, 6422.
29 M. He, L. Zhao, J. Wang, W. Han, Y. L. Yang, F. Qiu and Z. Q. Lin, *ACS Nano*, 2010, **4**, 3241.
30 M. He, W. Han, J. Ge, Y. L. Yang, F. Qiu and Z. Q. Lin, *Energy Environ. Sci.*, 2011, **4**, 2894.
31 M. He, W. Han, J. Ge, W. J. Yu, Y. L. Yang, F. Qiu and Z. Q. Lin, *Nanoscale*, 2011, **3**, 3159.
32 A. Yokoyama, R. Miyakoshi and T. Yokozawa, *Macromolecules*, 2004, **37**, 1169.
33 S. Cho, K. Lee, J. Yuen, G. M. Wang, D. Moses, A. J. Heeger, M. Surin and R. Lazzaroni, *J. Appl. Phys.*, 2006, **100**, 114503.
34 W. L. Ma, C. Y. Yang, X. Gong, K. Lee and A. J. Heeger, *Adv. Funct. Mater.*, 2005, **15**, 1617.
35 N. Overbergh, G. Smets and H. Berghman, *J. Polym. Sci., Part C: Polym. Symp.*, 1972, **38**, 237.
36 R. Tkachov, V. Senkovskyy, H. Komber, J. U. Sommer and A. Kiriy, *J. Am. Chem. Soc.*, 2010, **132**, 7803.
37 W. Yin and M. Dadmun, *ACS Nano*, 2011, **5**, 4756.
38 R. V. Castillo, A. J. Müller, J.-M. Raquez and P. Dubois, *Macromolecules*, 2010, **43**, 4149.
39 J. S. Huang, G. Li and Y. Yang, *Appl. Phys. Lett.*, 2005, **87**, 112105.
40 P. W. M. Blom, V. D. Mihailetchi, L. J. A. Koster and D. E. Markov, *Adv. Mater.*, 2007, **19**, 1551.
41 R. J. Kline, M. D. McGehee, E. N. Kadnikova, J. S. Liu, J. M. J. Frechet and M. F. Toney, *Macromolecules*, 2005, **38**, 3312.
42 V. D. Mihailetchi, H. X. Xie, B. de Boer, L. J. A. Koster and P. W. M. Blom, *Adv. Funct. Mater.*, 2006, **16**, 699.
43 H. Xin, X. G. Guo, F. S. Kim, G. Q. Ren, M. D. Watson and S. A. Jenekhe, *J. Mater. Chem.*, 2009, **19**, 5303.
44 P. Kohn, S. Huettner, H. Komber, V. Senkovskyy, R. Tkachov, A. Kiriy, R. H. Friend, U. Steiner, W. T. S. Huck, J. U. Sommer and M. Sommer, *J. Am. Chem. Soc.*, 2012, **134**, 4790.
45 O. F. Pascui, R. Lohwasser, M. Sommer, M. Thelakkat, T. Thurn-Albrecht and K. Saalwachter, *Macromolecules*, 2010, **43**, 9401.
46 Z. Y. Wu, A. Petzold, T. Henze, T. Thurn-Albrecht, R. H. Lohwasser, M. Sommer and M. Thelakkat, *Macromolecules*, 2010, **43**, 4646.
47 B. D. Olsen, M. Shah, V. Ganesan and R. A. Segalman, *Macromolecules*, 2008, **41**, 6809.
48 M. W. Matsen and C. Barrett, *J. Chem. Phys.*, 1998, **109**, 4108.
49 P. N. Murgatro, *J. Phys. D: Appl. Phys.*, 1970, **3**, 151.

50 T. Y. Chu and O. K. Song, *Appl. Phys. Lett.*, 2007, **90**, 203512.
51 A. J. Mozer and N. S. Sariciftci, *Chem. Phys. Lett.*, 2004, **389**, 438.
52 A. J. Mozer, N. S. Sariciftci, A. Pivrikas, R. Osterbacka, G. Juska, L. Brassat and H. Bassler, *Phys. Rev. B: Condens. Matter Mater. Phys.*, 2005, **71**, 035214.

53 T. J. Prosa, B. J. Bauer, E. J. Amis, D. A. Tomalia and R. Scherrenberg, *J. Polym. Sci., Part B: Polym. Phys.*, 1997, **35**, 2913.
54 J. D. Hoffman and J. I. Lauritzen, *J. Res. Natl. Bur. Stand.*, 1961, **65A**, 297.
55 M. Brinkmann and P. Rannou, *Adv. Funct. Mater.*, 2007, **17**, 101.